Insights into the structure and thermal stability of uranyl aluminate nanoparticles

Chave, T.; Le Goff, X.; Scheinost, A. C.; Nikitenko, S. I.;

Originally published:

January 2017

New Journal of Chemistry 41(2017), 1160-1167

DOI: https://doi.org/10.1039/c6nj02948e

Insights into the structure and thermal stability of uranyl aluminate nanoparticles

Tony Chave,[a]* Xavier Le Goff,[a] Andreas C. Scheinost,[b] and Sergey I. Nikitenko[a]

[a]Institut de Chimie Séparative de Marcoule (ICSM), UMR 5257 – CEA – CNRS – UM – ENSCM, Centre de Marcoule, BP 17171, 30207 Bagnols sur Cèze, Cedex, France

[b]Helmholtz Zentrum Dresden Rossendorf, Inst Resource Ecol, D-01314 Dresden, Germany

[*]E-mail: tony.chave@cea.fr; Fax:+33(0) 4 66 79 76 11 ; Tel:+33(0)4 66 33 92 50

Abstract

Ultrasonically assisted hydrolytic precipitation of U(VI) in the presence of mesoporous alumina followed by thermal treatment of solid precursor allowed to obtain crystallized uranyl aluminate (URAL) nanoparticles (NPs) dispersed in alumina matrix. Effect of U(VI) concertation and calcination temperature on the yield of URAL NPs was studied using XRD, XAFS and HRTEM techniques. At 800°C, URAL NPS (d≈5 nm) are formed only for low uranium loading of about 5 wt% whereas for higher content of uranium, larger U_3O_8 NPs (d≈20 nm) were identified as a principal uranium specie. At 500°C, URAL NPs are formed even for 25 wt% of uranium. U L_{III} edge EXAFS spectra pointed out that uranyl cation in URAL is coordinated by bidentate aluminate groups. Presumably URAL is formed during the heating of $2UO_3{\cdot}NH_3{\cdot}2H_2O$/AlO(OH) precursor. However, high temperature and larger content of uranium promote URAL transformation to more thermodynamically stable U_3O_8 oxide. This process is accompanied by uranium NPs growing via Ostwald ripening mechanism.

1. Introduction

Uranium is a naturally occurring element worldwide considered and involved in nuclear technology especially for electricity generation. This large industrial use raises many concerns regarding the reprocessing of spent nuclear fuel, the long-term nuclear waste disposals and the potential migration of uranium within the environment. It is in this context that many different topics related to uranium is actually ongoing.[1] Some studies are dedicated to existing uranium minerals occurring in the vicinity of natural uranium ore deposits in order to understand the long term behaviour and migration of uranium in a geological repository.[2-5] Other papers are related to the synthesis of new uranium compounds or to the migration of uranium species in water and their interaction in the geosphere by studying sorption complexes on natural oxides like silica, alumina or iron oxides or on various weathering products like aluminium hydroxide.[6-8] Corrosion and reprocessing of aluminium clad rod fuel is another topic of interest and also implies to understand the behaviour of uranium species in solution in the presence of alumina at various pH and especially in alkaline conditions at elevated temperature. [9-11]

Based on these issues, our previous work was dedicated to the interaction between alumina and uranyl ions under heating in order to demonstrate if the formation of uranyl aluminate (URAL) compounds was possible.[12] Noteworthy, uranyl aluminate complex cannot actually be directly

formed from the solution because uranyl is readily hydrolysed under alkaline conditions. Nevertheless, since uranyl ions can adsorb on various minerals and especially on alumina and gibbsite leading to formation of inner-sphere, bidentate complexes we believed that by promoting the dispersion of uranium within the system it may be possible to obtain uranyl aluminate compounds.[6, 7] Thus, in our previous study was reported for the first time the synthesis of URAL nanoparticles (NPs) within the range of several nanometres by hydrolytic precipitation of U(VI) at pH 11 in the presence of mesoporous alumina matrix exhibiting high specific surface area under 20 kHz ultrasonic irradiation followed by calcination at 800°C. Formation of URAL was notably confirmed by EXAFS analysis only for low concentration of uranium within the alumina matrix namely around 5 wt% of U. It was also observed that increasing uranium concentration to 30 wt% leads to the main formation of U_3O_8 at 800°C which is the expected thermodynamically stable uranium phase under such conditions. Finally, the EXAFS results suggested that uranyl cations are coordinated by bidentate aluminate groups. Nevertheless, thermal and concentration stability or URAL NPs as well its molecular structure remained to be addressed.

The present work is hence dedicated to fill this gap and will focus on the determination of the URAL formation mechanism and to give new insights on its structure and morphology by studying the products formed at different uranium concentrations in alumina matrix by coupling XRD, XAFS and High Resolution TEM analyses.

2. Experimental

Materials and reagents

Ammonia (28-30%) and hydrochloric acid (37%) solutions were purchased from Sigma Aldrich and Carlo Erba respectively and used without further purification. Wormhole like mesoporous alumina MSU-X type with a specific surface area previously measured around 259 $m^2.g^{-1}$ was also provided by Sigma Aldrich. All solutions were prepared using deionised water (Milli-Q system) with resistivity higher than 18.2 MΩ.cm at 25°C. Argon of 99.999% purity was provided by Air Liquide and used as gas atmosphere during all ultrasonic treatments. Solution of uranyl chloride (UO_2Cl_2) was prepared by dissolving the required amount of UO_3 within a small excess of HCl 37%. Uranium concentration in the various solutions was confirmed by ICP-OES analyses.

Ultrasonic irradiation

All experiments were carried within an air tight 50 mL double jacketed glass reactor insuring the control of both the gas atmosphere and the temperature during ultrasonic treatment. Ultrasonic irradiation was ensured by a piezoelectric transducer supplied by a 20 kHz electric generator (750W Sonics). The 1 cm^2 titanium ultrasonic horn was introduced reproducibly within 50 mL of solution. Prior ultrasonic treatment, argon was bubbled with a 100 mL/min flow rate for at least 15 min within the reaction medium and maintained during the experiment. The absorbed acoustic power P_{ac} ($W.mL^{-1}$) as well as the irradiation intensity I ($W.cm^{-2}$) were assessed using thermal probe method as previously described in the literature.[13] The sonochemical activity was also measured during the sonolysis of pure water under argon atmosphere by measuring the hydrogen peroxide formation rate using Ti(IV) dosimetry.[14] In our conditions, P_{ac} and I were respectively around 0.35 $W.mL^{-1}$ and 17 $W.cm^{-2}$ and the H_2O_2 formation rate under Ar atmosphere was determined to be 0.07 $\mu mol.min^{-1}$ at 20°C.

Sample preparation

Samples with different amount of uranium were synthesised based on the procedure previously reported in the litterature.[12] Typically, 300 mg of mesoporous alumina were suspended in 45 mL of UO_2Cl_2 solution with various concentrations under ultrasonic irradiation at pH 3.5±0.5 and 40±1°C. After a 30 min ultrasonic treatment, the pH of solution was increased to 11±0.5 with addition of 5 mL of 28% ammonia and left for 30 to 60 more minutes under ultrasound. The solid was then recovered by centrifugation, washed until neutral pH and dried overnight at room temperature under vacuum. Finally, samples were calcined under air at 500°C or 800°C during 5h with a heating rate of 5°C.min^{-1}. All samples prepared during this study are reported in Table 1 with estimated wt% of uranium in the final compound by taking into account that mesoporous alumina is partially soluble under ultrasound in basic conditions according to a previous study (20% in our conditions).[15]

Table 1: Composition and calcination temperature of URAL samples prepared during this study

Sample reference	m_{Al2O3} (mg)	m_U (mg)	wt% U added*	wt% U in matrix*	Calcination temperature (°C)	Sample colour
Al_2O_3	301.2	0	0	0	800	White
URAL 2.5%	301.2	6	2.5	2.4	800	Pale yellow
URAL 5%	300.2	12	5	4.8	800	Light yellow
URAL 10%	298.6	24	10	9.1	800	Pale green
URAL 15%	299.7	36	15	13.1	800	Light green
URAL 20%	301.6	48	20	16.6	800	Olive
URAL 25%	301.1	60	25	19.9	800	Green
URAL 25% 500°C	299.1	60	25	19.9	500	Orange

*based on the estimation that 20% of the initial mass of Al_2O_3 will be dissolved during ultrasonic treatment at pH=11.

Characterization methods

TEM. Obtained samples were dispersed in absolute ethanol within a 45 kHz ultrasonic bath (VWR). One drop of the suspension was then deposited on a carbon coated copper grid prior analysis with a JEOL 2200FS device for both low and high resolution characterization. Full size TEM images are given in ESI.

ICP-OES. Concentrations of uranyl chloride solutions were determined by ICP-OES analyses (Spectro ARCOS) following 5 specific emission wavelengths of uranium (329.133, 367.007, 385.958, 409.014 and 424.437 nm). The device was formerly calibrated with certified standard solutions (SCP Science) and all samples were diluted in 2% HNO_3 within the range of 0-15 ppm in order to meet the analysis requirements. Accuracy on the concentration determination was evaluated to be less than 5%.

SEM/EDX. Scanning electron microscopy measurements coupled with energy dispersive X-ray analysis (SEM/EDX) were done with a QUANTA FEG 200 ESEM scanning microscope. Samples were deposited on carbon tapes and analysed without any further preparation. Large field detector, involving secondary electrons, and backscattered electron observations were both carried out on the various synthesized samples.

XRD. All X-ray diffraction diagrams were obtained using a D8 Advance Bruker device equipped with a Cu Kα X-ray source (λ=1.5418 Å). Data were collected over a 2θ range of 10−100° using a step width of 0.01° and an acquisition time of 1 s per step for short time analysis to 3 s per step for long time acquisition. Analyses in temperature were also considered for the characterization of pristine mesoporous alumina, 5% and 25% URAL. Temperature increase was set to 2°C.min^{-1} and analyses were done every 100°C with an acquisition time of 1 h.

XAFS

XAFS measurements were performed on the Rossendorf Beamline (BM20-ROBL) at the European Synchrotron Radiation Facility (ESRF). This beamline is equipped with a Si(111) double monochromator and two platinum-coated mirrors for collimation and higher harmonics rejection. Energy calibration was achieved in regards to the first inflection point at 17038 eV of a yttrium metal foil. XAFS spectra were recorded at U L_{III} edge in transmission mode with energy threshold defined at 17185 eV. EXAFS data reduction and analysis were carried out using IFEFFIT software following standard procedures. Theoretical phase and amplitude functions were calculated with FEFF program. The amplitude reduction factor, S_0^2, in the FEFF calculation was defined as 0.9 and fixed to that value in the data fits.

3. Results and discussion

Depending on the amount of uranium initially added within the system, compounds with colours ranging from pale yellow (URAL 2.5%) to dark green (URAL 25%) were obtained after the ultrasonic treatment ultrasonic treatment and calcination at 800°C. Fig. 1 presents the powder XRD patterns obtained on URAL samples at 800°C from Al_2O_3 alone to 25% of uranium added. These results indicate that above an initially added amount of uranium of 5%, the presence of triuranium octaoxide (U_3O_8) can be pointed out on XRD patterns in agreement with the green colour of the samples. Formation of U_3O_8 under such conditions was expected since at the microscale this is a thermodynamically stable phase of uranium oxides.[16] For URAL 5%, which exhibits a yellow coloration, only a small amount of U_3O_8 can be actually identified but its signature is very weak and required a longer XRD acquisition time. No other specific diffraction peaks related to the presence of uranium could be pointed out in order to explain the colour observed for this sample. With a lower amount of incorporated uranium in the alumina matrix absolutely no traces of uranium oxide phases could be distinguished in the sample whatever the analysis conditions. Concerning the remaining diffraction peaks they can be attributed to various forms of alumina but mainly to γ-Al_2O_3 with also the presence of θ and η-Al_2O_3 which are typically observed after calcination of aluminium hydroxide, boehmite and γ-alumina oxide at 800°C (Fig. S1).[17] Pristine Al_2O_3 patterns show both sharp and quite large diffraction peaks which could be explained by a difference in crystallinity between the various Al_2O_3 allotropic forms or could results from the superposition of their respective contributions.

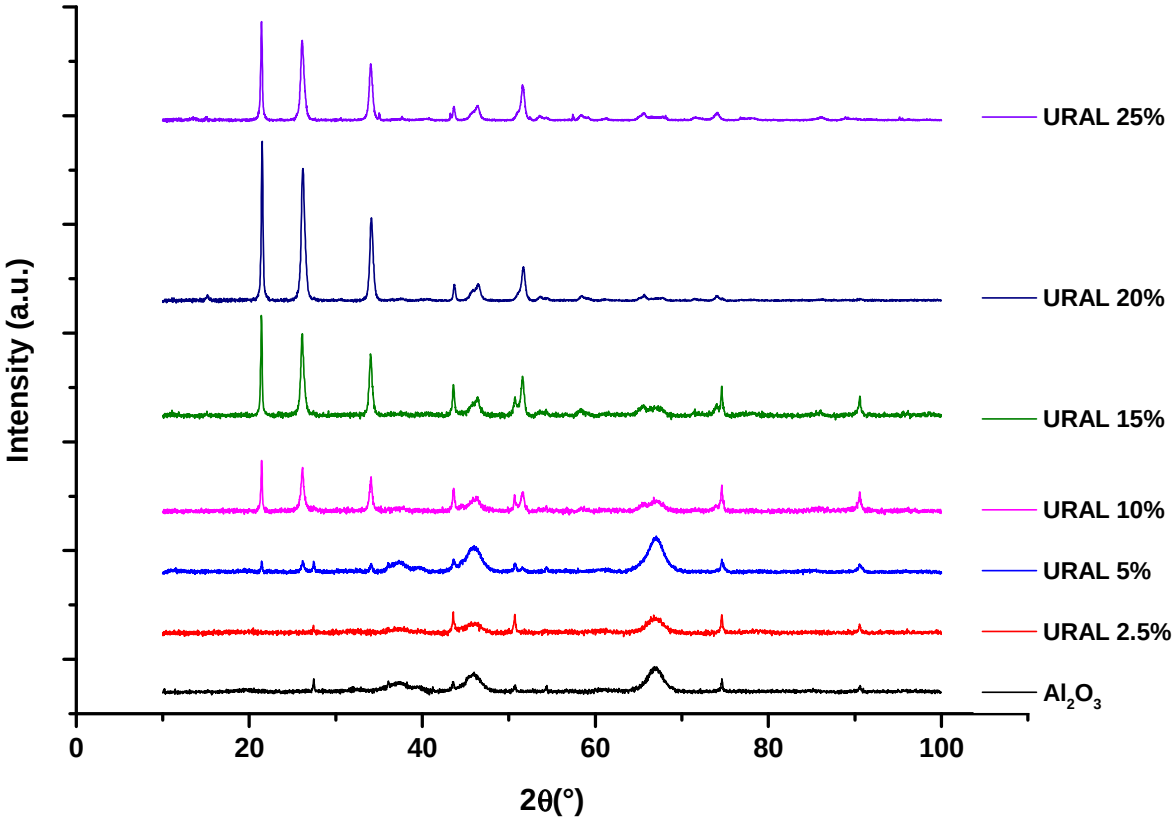

Fig. 1 XRD patterns obtained for URAL samples after ultrasonically assisted uranium precipitation and calcination at 800°C.

URAL samples were then analysed by SEM as shown on Fig. S2. Alumina matrix obtained after experimental procedure without addition of uranium exhibits quite heterogeneous particle sizes ranging from less than one micrometre to tens of micrometres. Addition of uranium solution during the ultrasonic treatment leads to similar results and doesn't significantly alter the sample mean particle size whatever the uranium concentration. X-Ray Energy dispersive analyses made on all URAL samples nevertheless confirmed the presence of uranium in all samples in various extents in agreement with the experimental procedure. However, for URAL samples with uranium amount higher than 10%, it is possible to observe that Al_2O_3 matrix is partially covered with small nodes of several hundreds of nanometres. SEM analyses carried out with backscattered electron detector actually reveal a phase contrast within the URAL samples only observed when larger amount of uranium is involved. As observed on Fig. S2 by comparing SE and BSE images of URAL 15% sample, the small particles located at the surface of the matrix appeared in BSE mode brighter than alumina support meaning they are mainly composed of heavier element, that is to say of uranium. According to XRD patterns shown in Fig. 1, it can be concluded that these dots are at least composed of U_3O_8 crystals for URAL samples with uranium content above 10%.

In view of better understanding the formation of uranium phases within the system, high temperature XRD characterizations were carried out on freshly prepared samples submitted to a 2°C.min^{-1} temperature increase starting from room temperature to 800°C with a XRD acquisition every 100°C. For the sample with low amount of uranium, no drastic evolution could be observed during the heat treatment and actually no uranium oxide phase could be pointed out (Fig. S3). Thermal evolution of URAL 25% was also considered and is reported in Fig. 2. It can be seen that at

room temperature uranium precipitated in the form of ammonium diuranate $2UO_3 \cdot NH_3 \cdot 3H_2O$.[16] This compound rapidly decomposes with the temperature increase and is almost not visible anymore at 200°C indicating the formation of amorphous uranium species until 600°C where U_3O_8 starts to crystallise in agreement with the litterature.[16]

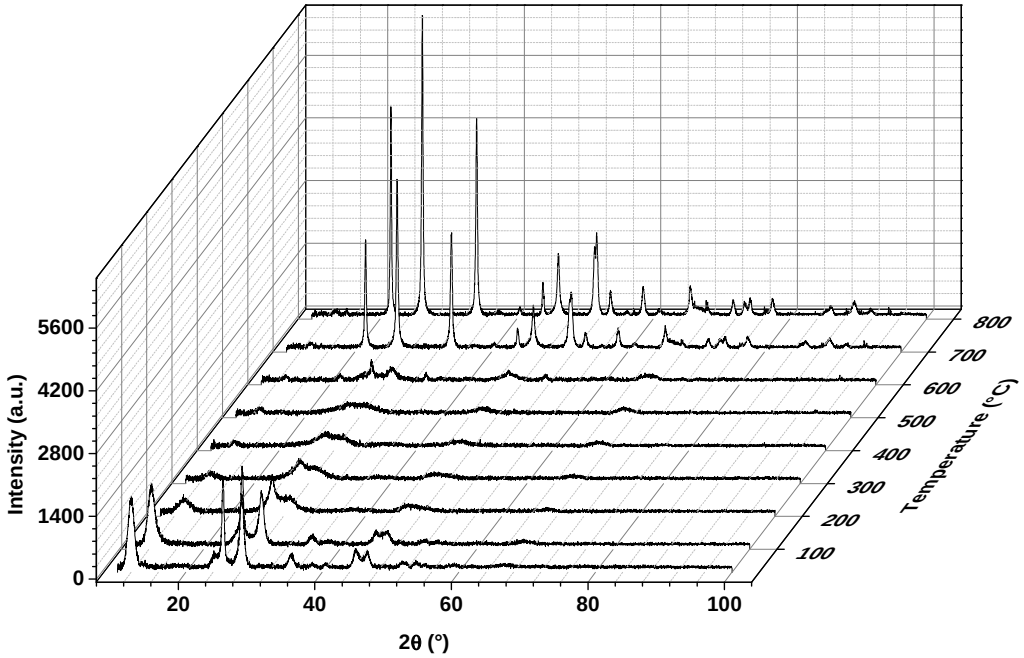

Fig. 2 XRD pattern evolution in temperature of URAL 25% sample prior calcination starting from 30°C to 800°C (from bottom to top)

Based on these results, we suggested that a new crystalized compound with 25% of uranium can be obtained by prolonged sample annealing at a temperature of 500°C instead of 800°C. Long time XRD survey of this sample reveals the presence of a new crystalline phase which was not observed at 800°C and low loading of uranium (Fig. 3). The XRD diagram of this specie exhibits broad diffraction peaks indicating the presence of very small uranium crystallites or low extent of crystallinity. According to the literature, ammonium diuranate calcination under air at 500°C should lead to amorphous or β-UO_3 phase.[16, 18, 19] However, XRD analysis shown in Fig. 3 revealed several specific diffraction peaks not observed for U_3O_8 or γ-Al_2O_3 phases which could be attributed to URAL with main corresponding d-spacings around 3.06 and 3.40 Å as observed in Fig. 3.

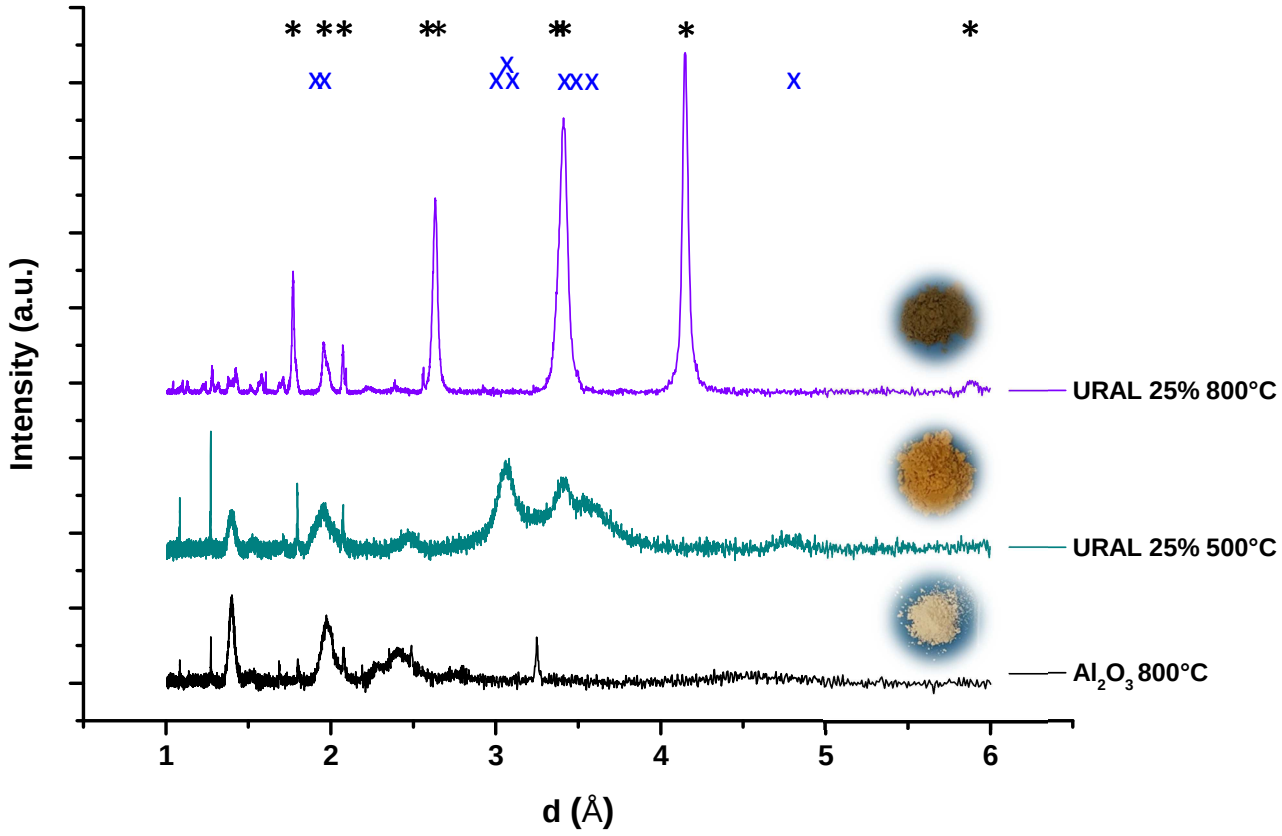

Fig. 3 Comparison of d-spacings obtained for alumina and URAL 25% heated at 800°C and 500°C. Black stars refer to α-U3O8 (PDF 00-047-1493) and blue crosses to β-UO_3 d-spacings (PDF 01-07-2124). In insets are given the pictures of the corresponding URAL samples.

Structural characterisation of the samples obtained at 800°C at various concentrations as well as the sample calcined at 500°C was performed by XAFS analyses. Both XANES and EXAFS spectra are given in Fig. 4. U-L_{III} edge XAFS analysis is actually a powerful tool for the determination of both the first neighbours and the oxidation state of uranium atom. In fact, as it can be seen from Fig. 4 (left), XANES spectra of URAL samples containing from 2.5% to 10 % of added uranium exhibit a shoulder on the right wing of the white line (arrow on Fig. 4), which arises from O=U=O multiple backscattering and is hence indicative of U(VI). The presence of uranyl unit in this compound is also confirmed by Fourier transforms (FT) of their EXAFS spectra which show a single backscattering peak at about 1.8 Å (peak A), followed by two longer U-O distances in the equatorial plane (peaks B and C). As seen in Fig. 4, the signature of uranyl group gradually disappears with increasing amount of added uranium within the URAL samples heated at 800°C. At the same time, a peak at about 4 Å becomes increasingly prominent (Fig. 4 E), in line with the U-U single scattering of U_3O_8 shown as a reference.

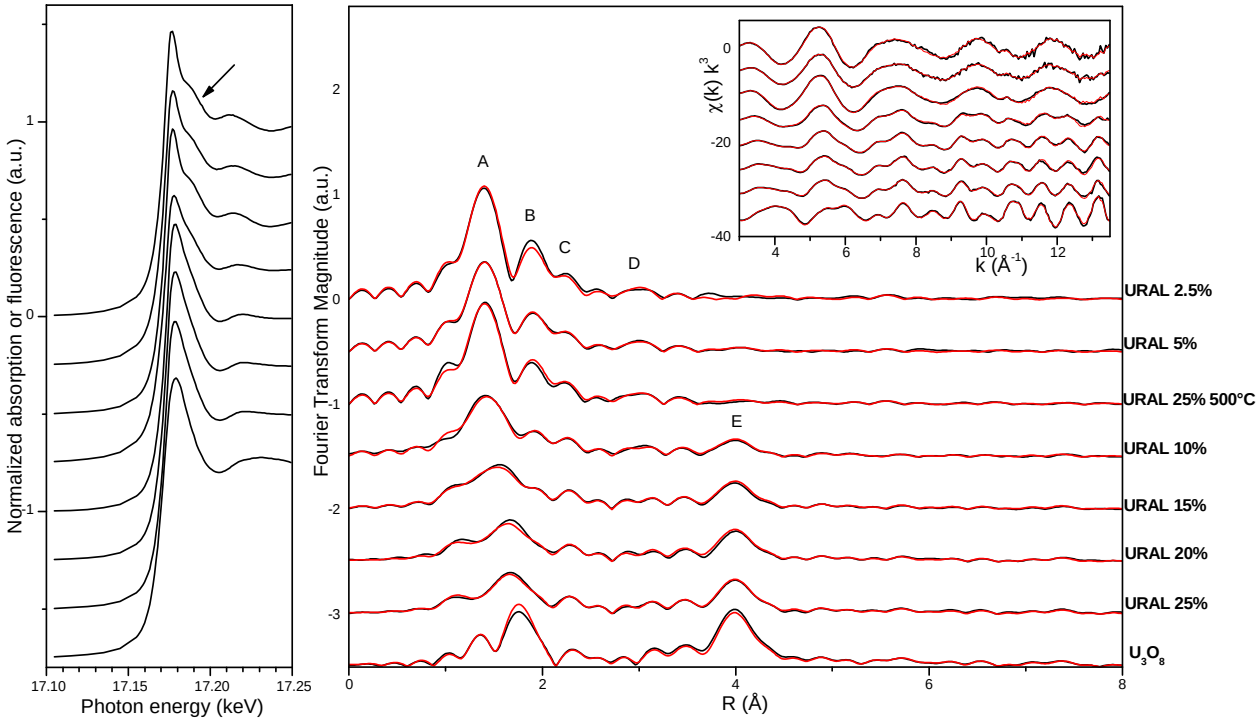

Fig. 4. U-L_{III} edge XANES (left) and the Fourier transforms uncorrected for the phase shift (right) of the k^3 weighted EXAFS spectra of URAL samples shown in the inset. Black lines are experimental data, red lines are reconstructed EXAFS data using two principal components.

In order to determine the number of uranium species present in the studied system, we performed a principal component analysis of the k3-weighted EXAFS spectra (2.0 to 14.5 $Å^{-1}$) using the ITFA program package.[20, 21] All URAL samples could be well-reconstructed using two components as observed with the fit of the EXAFS spectra in Fig. 4 (red lines). A further confirmation that only two structurally different U species are present comes from the Malinowsky indicator variable, which shows a minimum for two components, meaning that two principal components reconstruct the data with statistical significance. When adding the U_3O_8 reference spectrum to the data set, the minimum number of required principal components remained two, which necessarily means that the structure of U_3O_8 is a component of the sample spectra.

Furthermore, the VARIMAX factor loadings showed a monotonous decrease of factor 1 from URAL 2.5% to URAL 25% and then to U_3O_8 as well as a monotonous increase of factor 2 along this series (Fig. S4). This indicates that sample URAL 2.5% and the reference U_3O_8 constitute structural extremes, while the other samples are mixtures of these extremes. Table 2 shows the derived fractions 1 and 2 respectively related to uranyl aluminate and U_3O_8. Note that the fractions have not been normalized to a sum of unity, hence the sum reveals the error of the analysis, with a maximum deviation for sample URAL 5% of -11 %.

Table 2 ITFA-derived fractions of factors 1 and 2 using iterative transformation factor analysis.

Spectrum number	Sample reference	Fraction of Factor 1	Fraction of Factor 2	Sum
1	URAL 2.5%	1.00	0.00	1.00
2	URAL 5%	0.82	0.10	0.92
3	URAL 25% 500°C	0.91	0.10	1.01
4	URAL 10%	0.62	0.34	0.96
5	URAL 15%	0.47	0.53	1.00
6	URAL 20%	0.36	0.61	0.97
7	URAL 25%	0.34	0.65	0.99
8	U_3O_8	0.00	1.00	1.00

Table 3 summarizes the shell fit results of the two extreme components. URAL 25% was fitted with two axial oxygen atoms at 1.80 Å (peak A), and with five equatorial oxygen atoms of aluminate group in a split shell with distances of 2.33 and 2.46 Å (peaks B and C respectively). Taking into account the four-legged multiple backscattering contribution of the –yl unit (peak D), an additional 1.8 Al atoms could be fitted in this region, providing a distance of 3.60 Å. Distance and coordination number are indicative of a double-corner sharing arrangement between the equatorial oxygen atoms of the uranyl polyhedra and $Al(O,OH)_6$ octahedra. It is worth noting that the local structure of URAL obtained in this work is quite similar to that reported in our first communation.[4]

The U_3O_8 component was fitted using the neutron diffraction data of Andresen.[22] Note that the triplet FT peak of the first U-O interactions could not be fitted using distances and coordination numbers of this model. The best fit was obtained with a six-fold oxygen coordination of three different U-O distances, 1.94 Å, 2.13 Å and 2.28 Å, which vary significantly from the neutron diffraction distances of 2.07 Å (2-fold) and 2.18 Å (4-fold). In spite of these differences, our fit is still in line with hexacoordinated uranate local structure reported in the literature and with XAFS data obtained on α-U_3O_8 exhibiting also three similar U-O bond distances.[23, 24]

Table 3 EXAFS shell fit results ($S_0^2 = 0.9$).

Sample reference	Path	CN	R (Å)	σ^2 (Å²)	$\Delta E°$ (eV)	%R
URAL 2.5%	U-Oax	2.0	1.80	0.0024	13.8	12.7
	U-Oeq1	2.6	2.33	0.0061		
	U-Oeq2	2.4	2.46	0.0061		
	U-Al	1.8	3.60	0.0150		
U_3O_8	U-O1	0.8	1.94	0.0020	14.9	17.0
	U-O2	2.3	2.13	0.0020		
	U-O3	2.9	2.28	0.0020		
	U-O4	3.0	3.50	0.0066		
	U-U1	2.0	3.80	0.0057		
	U-U2	4.0	3.97	0.0048		
	U-U3	2.0	4.23	0.0025		

It is interesting to note that from sample URAL 5%, and so even for low amount of added uranium, the correct fit of EXAFS spectra required the contribution of U_3O_8 whose presence was confirmed by

XRD analyses (Fig. 1). In the same way, it can be seen from XAFS results that URAL 25% sample calcined at 500°C is definitively very similar to URAL 5% and 2.5% with a low U-U contribution at 4 Å. The fact that the U-U interaction remains low for URAL 25% 500°C implies that this compound doesn't consist in crystalline uranium oxides like UO_3, explaining the discrepancies observed during XRD analyses when comparing obtained pattern with β-UO3 reference.[19, 25, 26] These results also mean that uranyl aluminate samples with relatively large amount of uranium could be synthetized by reducing the calcination temperature to 500°C.

Calcined samples were then characterized by Transmission Electron Microscopy in order to characterize particle size and morphology of both U_3O_8 and URAL phases. Low resolution TEM analyses given in Fig. 5 reveal that alumina matrix obtained after ultrasonic treatment and calcination at 800°C (Fig. 5 A) consists in aggregates of 10 nm across particles. This result explains to a certain extent why obtained alumina XRD patterns exhibits quite large diffraction peaks. In Fig. 5 B and C, the presence of dark dots within the range of few nanometers can be observed along the alumina matrix which are certainly related to uranium compounds with high electron density. Moreover, in URAL samples with higher amount of uranium calcined at 800°C, bigger nanocrystals of tens of nanometers can be observed and the apparent phase contrast compared to alumina matrix clearly indicate that they are also composed of uranium which was confirmed by EDS analyses.

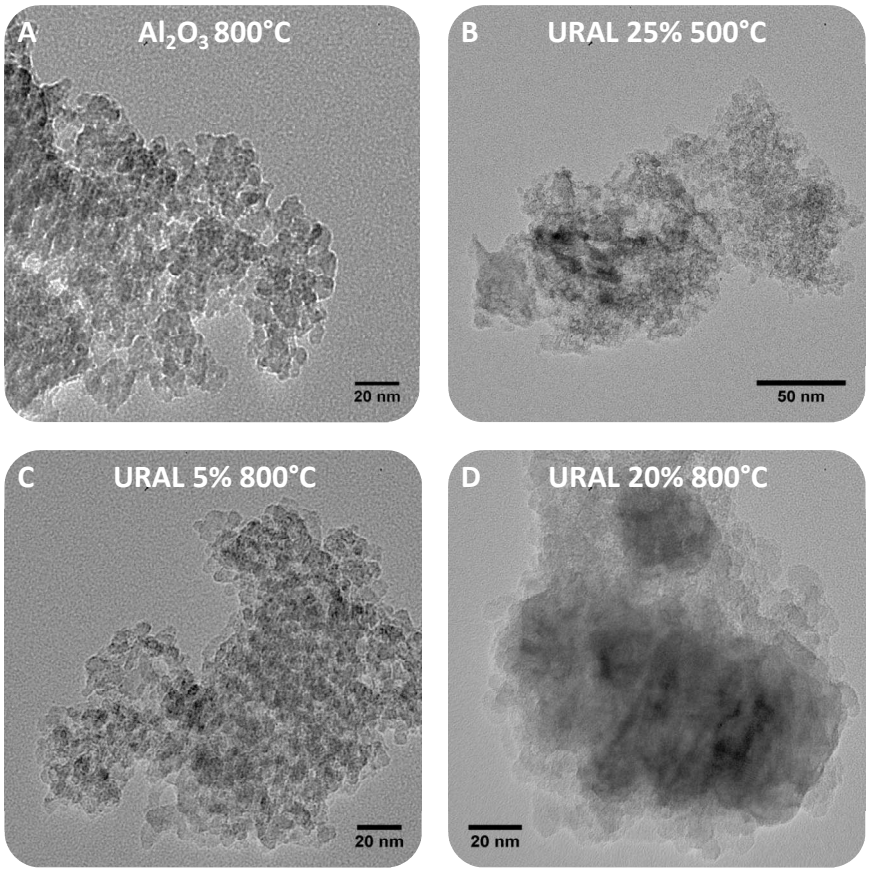

Fig. 5 Low resolution TEM images of URAL samples without uranium (A), with respectively 5% (C) and 20% uranium (D) after calcination at 800°C and URAL samples with 25% of added uranium calcined at 500°C (C)

High resolution TEM images of URAL 5% 800°C and URAL 25% 500°C reveal well-defined crystals with clearly seen d-spacing (Fig. 6). For URAL 25% 500°C, high resolution analyses confirms the presence of small crystallites below 5 nanometers with d-spacing in perfect line with what observed during

XRD characterization namely with value around 3.03 and 3.34 Å (Fig. 3). Noteworthy, Fig. 6 B points out that similar uranyl compounds could be observed in the URAL 5% 800°C sample among bigger crystals with larger d-spacing corresponding to U_3O_8 patterns in agreement with XRD analyses. According to PDF database, these d-spacing values observed in both samples and the corresponding XRD patterns actually do not match with any known uranium oxide stable at 800°C. In particular, this compound cannot refer to β-UO_3 since this phase is not stable at such temperature.[19]

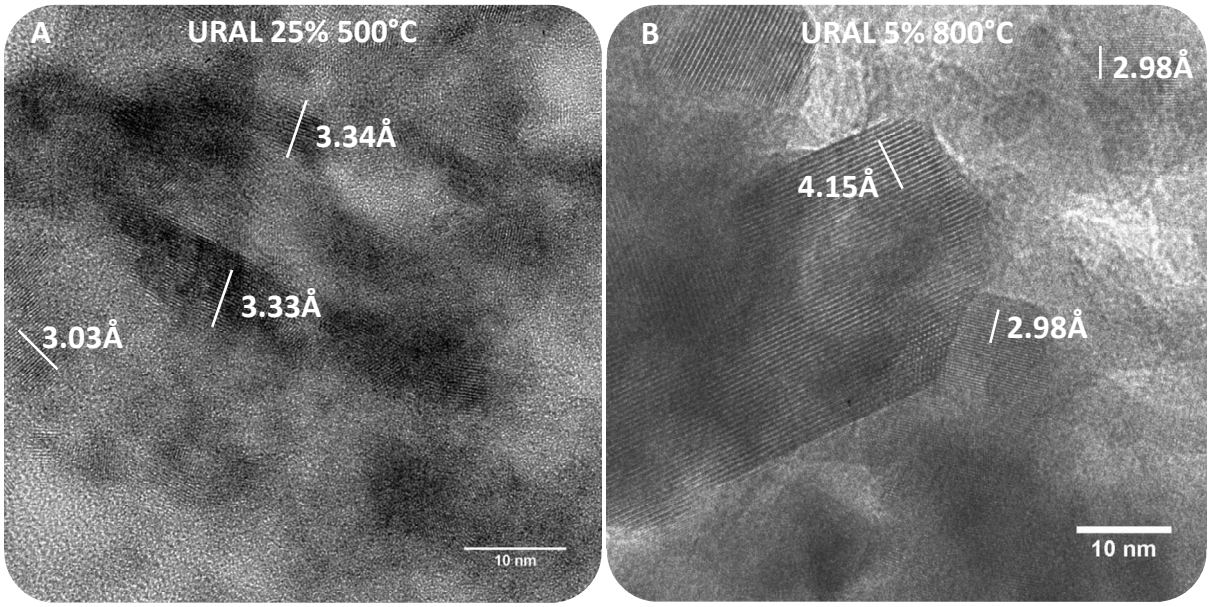

Fig. 6 High resolution TEM images of URAL 25% 500°C (A) and URAL 5% 800°C (B)

Based on HRTEM and XAFS analyses it is actually possible to confirm that the same uranyl compound is formed during the calcination of samples with 5% of uranium at 800°C and during the treatment at 500°C with 25% uranium content. Finally, the set of experimental results obtained in this work allows to suggest a mechanism of URAL formation shown in Fig. 7. At the first stage, ultrasonically assisted precipitation of ammonium diuranate provides highly dispersed uranium particles in alumina matrix and transformation of Al_2O_3 into more reactive boehmite AlO(OH) as it was recently reported.[1] Further heating of $2UO_3{\cdot}NH_3{\cdot}2H_2O$/AlO(OH) precursor up to 500°C leads to U(VI) interaction with aluminate groups instead of UO_3 formation. However, the efficiency of this process seems to depend strongly on the amounts or, in other words, on the particle surface density, of loaded uranium. At 800°C, uranium loading more than 2.5% probably promotes interparticle interaction via Ostwald ripening mechanism which causes formation of the thermodynamically more stable U_3O_8 species. This assumption is supported by the fact that U_3O_8 particles are larger compared to URAL particles.

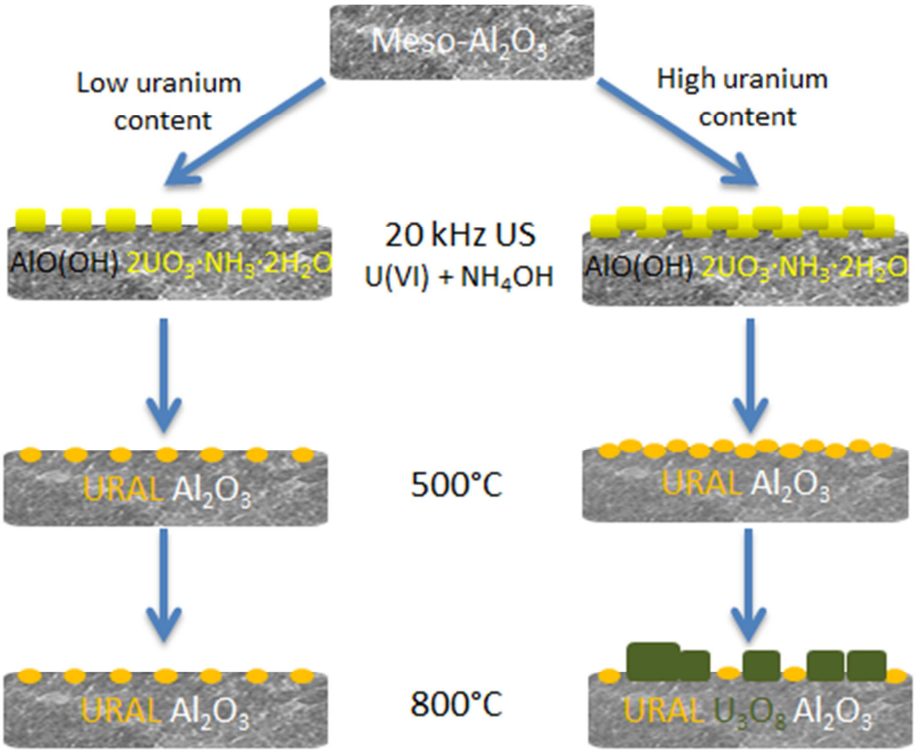

Fig. 7 Schematic representation of the URAL formation mechanism.

Conclusions

Based on our previous uranyl aluminate synthesis protocol, different samples with various amount of uranium ranging from 2.5 to 25% were synthesized and calcined at 800°C. XAFS analyses carried out on all URAL samples clearly indicate the presence of uranyl aluminate in all samples with increasing amount of U_3O_8 above a uranium content of 5%. High temperature diffraction of URAL 25% points out a transition temperature between the complete degradation of ammonium diuranate compound precipitated at room temperature and the formation of U_3O_8 thermodynamic stable phase at 800°C. A new URAL sample with a uranium content of 25% but a calcination temperature of 500°C was therefore synthetized. According to EXAFS analysis, this last sample proves to be very similar to low uranium content samples calcined at 800°C with the presence of uranyl and a very low U-U interaction. By coupling XRD and High Resolution TEM analyses it was then possible to confirm the presence of the same uranyl compounds within samples obtained at 500°C and 800°C. In the same way, EXAFS shell fit results are actually in line with our previous work and indicate that URAL can be described as uranyl cation coordinated with bidentate aluminate groups. TEM characterizations also reveal that uranyl aluminate particles consist in few nanometres crystallites where as U_3O_8 phase exhibits bigger particle size around tens of nanometres. Due to the small particle size of URAL compounds, obtained XRD patterns exhibit large diffraction peaks and no detailed structure could be established. This study allowed us to propose a formation mechanism and also to demonstrate the synthesis of nanocrystalline uranyl aluminate particles with high uranium content. Finally, it should be emphasized that to the best of our knowledge uranyl aluminate is a first example of chemical compound which can be obtained only as nanocrystals.

Acknowledgements

The authors thank H-P. Brau for TEM analyses and J. Ravaux for SEM/EDS characterizations.

References

1. B. J. Merkel and A. Hasche-Berger, *Uranium in the Environment*, Springer, Berlin, 2006.
2. T. Sato, T. Murakami, N. Yanase, H. Isobe, T. E. Payne and P. L. Airey, *Environ. Sci. Technol.*, 1997, **31**, 2854-2858.
3. J. L. Jerden, A. K. Sinha and L. Zelazny, *Chem. Geol.*, 2003, **199**, 129-157.
4. G. R. Lumpkin, *Journal of Nuclear Materials*, 2001, **289**, 136-166.
5. R. Metcalfe and C. A. Rochelle, *Chemical Containment of Waste in the Geosphere* The Geological Society London, 1999.
6. E. R. Sylwester, E. A. Hudson and P. G. Allen, *Geochim Cosmochim Ac*, 2000, **64**, 2431-2438.
7. T. Hattori, T. Saito, K. Ishida, A. C. Scheinost, T. Tsuneda, S. Nagasaki and S. Tanaka, *Geochim Cosmochim Ac*, 2009, **73**, 5975-5988.
8. L. Candela, I. Vadillo, P. Aagaard, E. Bedbur, M. Trevisan, M. Vanclooster, P. Viotti and J. A. López-Geta, *Water Pollution in Natural Porous Media at Different Scales. Assessment of Fate, Impact and Indicators. WAPO2*, Instituto Geológico y Minero de Espana, Madrid, 2007.
9. M. D. Kaminski and M. M. Goldberg, *Journal of Nuclear Materials*, 2002, **304**, 182-188.
10. C. T. Johnston, S. F. Agnew, J. R. Schoonover, J. W. Kennedy, B. Page, J. Osborn and R. Corbin, *Environ. Sci. Technol.*, 2002, **36**, 2451-2458.
11. *Corrosion of Research Reactor Aluminium Clad Spent Fuel in Water*, Technical report series N°418, IAEA, Vienna, 2003.
12. T. Chave, S. I. Nikitenko, A. C. Scheinost, C. Berthon, B. Arab-Chapelet and P. Moisy, *Inorganic Chemistry*, 2010, **49**, 6381-6383.
13. S. I. Nikitenko, C. Le Naour and P. Moisy, *Ultrason. Sonochem.*, 2007, **14**, 330-336.
14. D. W. O'Sullivan and M. Tyree, *International Journal of Chemical Kinetics*, 2007, **39**, 457-461.
15. T. Chave, S. I. Nikitenko, D. Granier and T. Zemb, *Ultrason. Sonochem.*, 2009, **16**, 481-487.
16. R. Eloirdi, D. Ho Mer Lin, K. Mayer, R. Caciuffo and T. Fanghänel, *Journal of Materials Science*, 2014, **49**, 8436-8443.
17. P. S. Santos, H. S. Santos and S. P. Toledo, *Materials Research*, 2000, **3**, 104-114.
18. P. Debets, *Acta Crystallographica*, 1966, **21**, 589-593.
19. H. R. Hoekstra and S. Siegel, *Journal of Inorganic and Nuclear Chemistry*, 1961, **18**, 154-165.
20. A. Rossberg, T. Reich and G. Bernhard, *Anal Bioanal Chem*, 2003, **376**, 631-638.
21. A. C. Scheinost, A. Rossberg, D. Vantelon, I. Xifra, R. Kretzschmar, A. K. Leuz, H. Funke and C. A. Johnson, *Geochim Cosmochim Ac*, 2006, **70**, 3299-3312.
22. A. F. Andresen, *Acta Crystallographica*, 1958, **11**, 612-614.
23. A. L. Tamasi, K. S. Boland, K. Czerwinski, J. K. Ellis, S. A. Kozimor, R. L. Martin, A. L. Pugmire, D. Reilly, B. L. Scott, A. D. Sutton, G. L. Wagner, J. R. Walensky and M. P. Wilkerson, *Analytical Chemistry*, 2015, **87**, 4210-4217.
24. L. R. Morss, N. M. Edelstein and J. Fuger, *The chemistry of the actinide and transactinide elements*, Springer Netherlands, 2011.
25. G. C. Allen, P. A. Tempest, C. D. Garner, I. Ross and D. J. Jones, *J Phys Chem*, 1985, **89**, 1334-1336.
26. G. N. Greaves, N. T. Barrett, G. M. Antonini, F. R. Thornley, B. T. M. Willis and A. Steel, *J Am Chem Soc*, 1989, **111**, 4313-4324.